X-rays from Solar Wind Charge Exchange at Mars: A Comparison of Simulations and Observations

H. Gunell and M. Holmström

Swedish Institute of Space Physics, Kiruna, Sweden

E. Kallio and P. Janhunen

Finnish Meteorological Institute, Helsinki, Finland

K. Dennerl

Max-Planck-Institut für extraterrestrische Physik, Garching, Germany

A hybrid simulation of the solar wind-Mars interaction and a test particle simulation of heavy ion trajectories near Mars are used to compute the contribution from solar wind charge exchange processes to the X-ray emission from Mars. It is found that the X-ray halo observed by the Chandra X-ray observatory can be explained by emissions from heavy, highly charged, ions in the solar wind undergoing charge exchange collisions in the upper atmosphere of Mars.

1. Introduction

There are several possible mechanisms for X-ray generation in the atmosphere and exosphere of Mars. Three of the proposed mechanisms are fluorescence and scattering of solar X-rays; electron bremsstrahlung and line emissions; and solar wind charge-exchange.

Fluorescence by solar X-rays occur when photons are absorbed by atmospheric neutrals and then re-emitted isotropically. Solar X-rays can also be elastically scattered by atmospheric neutrals. A detailed, quantitative, analysis of the intensity of the X-rays produced by these two mechanisms has been done by *Cravens and Maurellis* [2001]

Bremsstrahlung and line emissions result when neutrals that are photo-ionized interact with the solar wind plasma and excite waves, that in turn can accelerate electrons to keV energies. When such electrons collide with neutrals, X-rays can be produced by bremsstrahlung and K-shell radiation. This mechanism has been proposed for cometary X-rays [*Bingham et al.*, 1997; *Shapiro et al.*, 1999], but could also take place at Mars.

The third mechanism is solar wind charge exchange (SWCX). Wherever the solar wind meets a neutral atmosphere, X-rays are emitted by a charge exchange process between the neutrals and heavy solar wind ions. A small fraction of the solar wind consists of heavy, multiply charged ions such as O^{6+}, C^{6+} and Ne^{8+}. Charge-exchange between such an ion and a neutral atom can leave the ion in an excited state. When the captured electron then transits to a lower energy state, within the L- and K-shells, X-rays may be emitted. This source of X-rays was first proposed by *Cravens* [1997] as an explanation of X-rays observed from comets, and probably this process is the dominant source of the soft X-ray emissions from comets [*Cravens*, 2002]. It was then suggested by *Cravens* [2000] and *Krasnopolsky* [2000] that this should be a source of X-ray emissions also at Mars. Computer simulations of the intensities and morphology of these emissions was presented by *Holmström et al.* [2001] for Mars.

In recent years there have been observations of planetary X-ray emissions. X-rays from Venus [*Dennerl et al.*, 2002] and Mars [*Dennerl*, 2002] were discovered using the Chandra X-ray observatory.

When Mars was observed in 2001, *Dennerl* [2002] found that the X-ray emission from a disk the size of Mars was dominated by fluorescent scattering of solar X-rays. A faint X-ray halo surrounding the disk was also detected. The X-ray spectrum of the halo differed from that of the disk, and cannot be explained by fluorescence. The fluorescence peak at 0.65 keV, that is seen in the emissions from the disk, is absent in the X-ray emissions from the halo, c.f., figure 4 of [*Dennerl*, 2002]. Fluorescence is an efficient process only at low altitudes. *Dennerl* [2002] suggested that the halo could be caused by the SWCX process. In this work we perform a computer simulation to enquire whether charge exchange processes can explain the Martian X-ray halo.

In the future, imaging of SWCX could provide information on exospheric densities, solar wind composition and solar wind conditions. Since the imaging is global, we can get instantanous information on the conditions in the whole near Mars environment. To extract the information from images of the X-ray flux, detailed modeling of the production process will be needed, as discussed in [*Holmström and Kallio*, 2004].

2. Simulation Model

Here we present the method by which we have produced simulated images of SWCX at Mars that corresponds to the observation by Chandra in 2001.

The calculations were performed in three steps. First the solar wind parameters were estimated from data obtained by the WIND spacecraft. Since Mars was near opposition the plasma that was sampled by WIND near the earth on July 2, 2001 arrived at Mars two days later during the X-ray observation. The data was scaled with the distance from the sun, and the average parameter values over the period of the observation were used as input parameters for a hybrid simulation. These parameters are: $v_{sw} = 330$ km/s; $n_{sw} = 4.40 \times 10^6 \mathrm{m}^{-3}$; $T_{p,sw} = 4.56 \times 10^4$ K; and $\vec{B} = (1.13, -3.63, 0)\mathrm{nT} = 3.80\mathrm{nT} \cdot (\cos(72.7^\circ), -\sin(72.7^\circ), 0)$.

The parameters are estimated in the following way. The arrival time at Mars of a particular plasma element as a function of the time it passed by the earth was calculated from the v_x data. This gives an interval, starting at 00:57:49 (UT) and ending 18:49:49 (UT) on July 2, over which the plasma

0094-8276/04/$5.00

parameters are averaged. The plasma that passed the earth during this interval reach Mars during the observation two days later. We use a Mars-centred coordinate system with the sun in the positive x-direction, a northernly z-axis that is perpendicular to the ecliptic, and a y-direction that closes the right-handed system. The solar wind speed v_{sw} and the proton temperature $T_{p,sw}$ are assumed to be constants, and are simply the average values of v_x and T_p. The density n_{sw} and the magnitude of the magnetic field $|B|$ are scaled by the squared ratio of the two planets respective distances from the sun: $n_{sw} = n_p/1.446^2$ and $B_{sw} = B/1.446^2$. The z-component of the magnetic field is smaller than the other two for most of the observation, and therefore $B_z = 0$ is assumed. We have assumed that the the direction of the magnetic field is given by a a Parker-spiral, which means that B_y/B_x is proportional to the distance from the sun.

The second step was running a hybrid simulation of the interaction between the solar wind and Mars [*Kallio and Janhunen*, 2001, 2002] to obtain the electric and magnetic fields around Mars at the time of the observation. The hybrid code was run using 1.7×10^6 particles, with a fully absorbing obstacle boundary at $R_{\rm obst} = 3600$ km. The simulation box was a Mars-centred $6R_{\rm obst} \times 6R_{\rm obst} \times 6R_{\rm obst}$ cube. A grid with three different cell sizes, namely $0.05R_{\rm obst}$, $0.1R_{\rm obst}$, and $0.2R_{\rm obst}$, was used. The smallest cells were used close to the planet on the dayside.

As a third step a test particle simulation was run, calculating the trajectories of heavy solar wind ions in the electric and magnetic fields that were obtained from the hybrid simulation, and for each time step of the test particle simulation saving the X-ray emission density on a grid. The trajectories were compued by integrating the Lorentz force using Boris' CYLRAD algorithm (see for example *Hockney and Eastwood* [1988]) One hundred thousand trajectories were calculated for each of the ion species O^{7+}, C^{6+}, O^{6+}, O^{8+}, Mg^{10+}, Mg^{9+}, Si^{9+}, N^{6+}, C^{5+}, Ne^{8+}, Fe^{9+}, S^{9+}, Si^{8+}, Fe^{11+}, and Mg^{8+}. These species were selected from table 1 of *Schwadron and Cravens* [2000] for being the ion species that generate the highest luminosity, and together comprising 91.6 % of the total luminosity of the species of in that table. The test particles were injected in the simulation box of the hybrid simulation at its upstream edge. The initial velocity distribution was assumed to be a Maxwellian with temperature $T_{p,sw}$ that is centred around the drift speed v_{sw}, i.e., we assume that all species have the same temperature and that that temperature is equal to the temperature of the solar wind protons.

The cross sections for charge exchange (σ), the relative abundance of each ion species in the solar wind (a), and the energy released ($E_{n\rightarrow n_0}$) were taken from table 1 of *Schwadron and Cravens* [2000]. The cross sections reported by *Schwadron and Cravens* [2000] are for charge exchange collisions between heavy ions and water molecules, but since the ionisation potential for O, H, and H_2 are close to that of water using the cross sections for water is a reasonable approximation [*Wegmann et al.*, 1998]. An excited ion may go through several intermediate states before reaching the ground state, and thus release its energy to several photons. We use a simplified model, assuming that the transition to the ground state occurs in either one or two steps [*Schwadron and Cravens*, 2000]. Neutral exosphere densities for atomic oxygen and hydrogen and molecular hydrogen for solar maximum conditions were used [*Kallio et al.*, 1997; *Krasnopolsky and Gladstone*, 1996]. The densities are modelled by a Chamberlain exosphere [*Chamberlain and Hunten*, 1987], which is a spherically symmetric model. The exobase altitude is 170 km, and the exobase densities are $n_H = 3.1\times10^{10}\mathrm{m}^{-3}$ for atomic hydrogen, $n_{H_2} = 4.3\times10^{11}\mathrm{m}^{-3}$ for molecular hydrogen, and $n_O = 3.3\times10^{14}\mathrm{m}^{-3}$ for atomic oxygen. The exobase conditions (temperature and density) has large temporal and spatial variation [*Keating et al.*, 1998], resulting in large variations of exospheric densities.

Each test particle represents a large number of solar wind ions, and this number decreases as the test particle moves through the simulation area, where some of the real particles it represents are lost in charge exchange collisions. The density n_i represented by a test particle is

$$n_i(s) = n_{sw} a e^{-\sigma \int_0^s N_i(s')ds'} \quad (1)$$

where n_{sw} is the solar wind proton density, s the path length along the trajectory, $N_i(s)$ the density of the neutral exosphere, and a is the relative abundance of the particular ion species in the solar wind, i.e., $a = n_i(0)/n_{sw}$. The contribution from one test particle to the density of the emitted X-ray power is then

$$\begin{aligned} P_i(s) &= -\frac{dn_i}{dt} E_{n\rightarrow n_0} \\ &= n_{sw} a \sigma N_i(s) v_i(s) e^{-\sigma \int_0^s N_i(s')ds'} E_{n\rightarrow n_0} \end{aligned} \quad (2)$$

For each test particle at each time step this is accumulated on a grid, in a way that is analogous with the way charge is assigned to a grid in a particle in cell simulation. The total emitted X-ray power density is then found by summation of the contributions from all ion species.

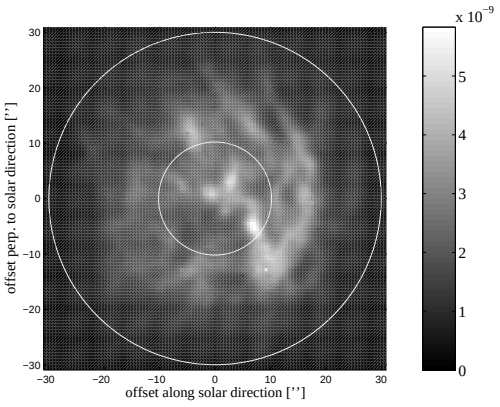

Figure 1. A simulated X-ray image of Mars at a phase angle of 18.2°, corresponding to the situation at the time of the observation. The inner white circle, with radius 10.2 arc seconds, marks the geometric size of Mars, and the outer white circle, with radius 30 arc seconds marks the extent of the X-ray halo according to *Dennerl* [2002]. The grey-scale shows the X-ray radiance in $\mathrm{Wm}^{-2}\mathrm{sr}^{-1}$.

Ions can, in principle, undergo several charge exchange collisions until they have lost all their charge, emitting photons in each step. This means that O^{7+} ions after a charge exchange collisions are a source of O^{6+} ions. We have neglected this source term after examining the exponential function $\exp(-\sigma \int_0^s N_i(s')ds')$ of Eq. (1). The value of the exponential when a test particle leaves the system, either by precipitating on the atmosphere or by leaving the outer boundary of the simulation box, is a measure of what fraction of the original density that still remains. If the value of the exponential still is close to unity when the particles leave the system the traversed region of the atmosphere can be considered collisionally thin and the additional source term is negligible. The average value of this factor computed using ten thousand test particles of the most important species, i.e., O^{7+} and C^{6+}, is 0.85 and 0.92 respectively. The worst case would be the species with the highest cross section, which in our case is Fe^{11+} for which $\sigma = 1.5 \times 10^{-18} m^2$. For Fe^{11+} the average value of the exponential is 0.82 for particles leaving the system. We thus find it justified to neglect this small ion source.

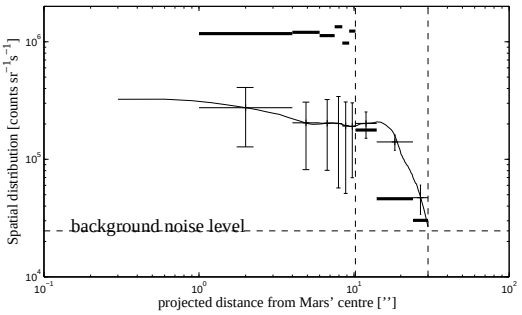

Figure 2. Radial distribution of the observed X-ray intensity in units of $sr^{-1}s^{-1}$. The thin solid curve shows the results of the simulation. The horizontal thick lines are a histogram of the observed X-ray photons. The horizontal thin lines show the average X-ray intensity in the same intervals as the histogram of the observation. The error bars mark a 90% confidence interval of the simulated results, assuming a Poisson distribution for the count rate. The vertical dashed lines mark the size of Mars and the extent of the X-ray halo according to *Dennerl* [2002], i.e., these lines correspond to the circles of Fig. 1.

3. Results

The flux that can be observed by an observer at earth is found by integration along lines of sight. Since the observer is very far away we use a parallel projection. $p(\xi,\zeta) = 1/(4\pi) \int P(x,y,z)ds$ is the directional X-ray energy flux measured in watts per square metre and steradian. ξ corresponds to the offset along the solar direction and ζ to the offset perpendicular to the solar direction. Fig. 1 shows the directional X-ray energy flux from Mars. The inner white circle, with radius 10.2 arc seconds, marks the geometric size of Mars, and the outer white circle, with radius 30 arc seconds marks the extent of the X-ray halo according to *Dennerl* [2002]. The grey-scale shows the X-ray radiance in $Wm^{-2}sr^{-1}$. In Fig. 1 we have included only photons with energies above 200 eV. The photon energy is modelled, following *Schwadron and Cravens* [2000], under the assumption that an ion in its excited state (quantum number n) emits its energy, $E_{n\to n_0}$, in either one or two steps, and that all transitions have an equal probability given by $1/(n-n_0)$. The quantity shown in Fig. 1 is thus

$$p_E(\xi,\zeta) = \frac{S v_{sw} n_{sw}}{4\pi} \int \sum_{species} \frac{a\sigma\Lambda}{N_{tp}} \sum_{E_{ph}>E} \frac{E_{ph}}{n-n_0} ds$$

where S is the cross section of the simulation box, E_{ph} is the photon energy, and $E = 200$ eV is the minimum energy of the photons included in Fig. 1. For $E = 0$, that is, if all photons are included, $p_E(\xi,\zeta) = p(\xi,\zeta)$.

To be able to compare with observations the energy dependent effective detector area $A(E_{ph})$ has to be taken into account. The observed directional flux expressed as a count rate is

$$c_{AE}(\xi,\zeta) = \frac{S v_{sw} n_{sw}}{4\pi} \int \sum_{species} \frac{a\sigma\Lambda}{N_{tp}} \sum_{E_{ph}>E} \frac{A(E_{ph})}{n-n_0} ds$$

The radial distribution of the X-ray power is shown in Fig. 2, where the thin solid curve displays the quantity

$$f(\rho) = \frac{1}{2\pi} \int_0^{2\pi} c_{AE}(\rho,\varphi) d\varphi \qquad (3)$$

where ρ is the radial and φ is the azimuthal polar coordinate of Fig. 1. The thick horizontal lines in Fig. 2 are a histogram of the observed X-ray photons. To facilitate a comparison between the simulation and the observation averages of the simulated curve, obtained from Eq. (3), over the same radial bins as those used for the observed photons, are shown as thin horizontal lines. The error bars show the limits of a 90% confidence interval of what would have been observed from our simulation, assuming a Poisson distribution for the count rate. The probability of observing a count rate smaller than the lower limit is 5% and that of observing a count rate higher than the upper limit of the error bar is also 5%.

The luminosity of the halo reported by *Dennerl* [2002] in the energy range $E = 0.5 - 1.2$ keV is 0.5 ± 0.2 MW. In this energy range the present simulation yields a luminosity of 1.8 MW. This figure is obtained by integrating all emissions within the simulation box.

4. Conclusions

We have reported simulations of X-ray emissions from Mars caused by the solar wind charge exchange process. Previous observations of Martian X-rays show a high count

rate of photons from a disk of the size of the planet and lower count rates from an X-ray halo surrounding it. The emissions from the disk were interpreted as fluorescent scattering of solar X-rays. The photon flux calculated here is substantially lower than that observed from the disk (Fig. 2), which is what should be expected since we only calculate the charge exchange contribution. For the halo the calculated count rates are higher than those that were observed by a factor between one and three.

There are a few uncertainties of the model that could contribute to this discrepancy. First, the density of the neutral exosphere of Mars changes with the solar cycle, and the estimate we used for solar maximum conditions might be incorrect for the particular time of observation. Secondly, the estimate of the solar wind parameters might be inaccurate, since it was based on measurements near Earth and relies on the solar wind conditions being unchanged over an angle of 6°. Thirdly, the composition of the solar wind, i.e. the abundances of the heavy ions, may, on the day of the observation, have differed from the estimates we used. Fourthly the fields obtained from the hybrid simulation may be inaccurate due to the limited spatial resolution. The hybrid model reproduces the basic plasma and magnetic field regions around Mars that were measured by the Phobos-2 mission, for example the bow shock, magnetotail, and how the magnetic field is piled up against the planet [*Kallio and Janhunen*, 2001, 2002]. Fifthly there could be errors in the values that we have used for the charge exchange cross sections. The classical over-barrier cross sections this we have used are generally over-estimates, and that can contribute to the discrepancy between the between the measured and simulated halo emissions.

In addition to the overall discrepancy it can be seen in Fig. 2 that the discrepancy between the simulations and the observations is the largest for the second bin of the halo. This can indicate that the radial dependence of the neutral exosphere model deviates from the actual exospheric density on the day of the observations. In this way X-ray observations can provide a means of studying the radial dependence of the exosphere density. In a forthcoming paper [*Gunell et al.*, 2004] we will investigate what influence fluctuations in the different parameters have on the observed X-ray emissions.

These simulations show that the contribution from the solar wind charge exchange process to the X-ray emissions from the halo is large enough to explain the observed X-ray flux.

5. Acknowledgement

We are grateful to Ronald P. Lepping (NASA/Goddard SFC) for the WIND MFI data, and to K.W. Ogilvie (NASA/GSFC), A.J. Lazarus (MIT), and J.C. Kasper (MIT) for the WIND SWE data. This work was supported by the Swedish National Space Board.

References

Bingham, R. J., M. Dawson, V. D. Shapiro, D. A. Mendis, and B. J. Kellet, Generation of X-rays from comet C/Hyakutake 1996 B2, *Science*, *275*, 49–51, 1997.

Chamberlain, J. W., D. M. Hunten, Theory of planetary atmospheres, 2nd Edition. Academic Press, inc., San Diego, California, 1987.

Cravens, T. E., Comet Hyakutake x-ray source: Charge transfer and solar wind heavy ions, *Geophys. Res. Lett.*, *24*, 105–108, 1997.

Cravens, T. E., X-ray emission from comets and planets, *Adv. Space Res.*, *26*(10), 1443–1451, 2000.

Cravens, T. E., X-ray emission from comets, *Science*, *296*, 1042–1045, 2002.

Cravens, T. E., and A. N. Maurellis, X-ray emission from scattering and fluorescence of solar x-rays at venus and mars, *Geophys. Res. Lett.*, *28*(15), 3043–3046, 2001.

Dennerl, K., Discovery of X-rays from Mars with Chandra, *Astronomy & Astrophysics*, *394*, 1119–1128, doi:10.1051/0004-6361:20021116, 2002.

Dennerl, K., V. Burwitz, J. Englhauser, C. Lisse, and S. Wolk, Discovery of X-rays from Venus with Chandra, *Astronomy & Astrophysics*, *386*, 319–330, doi:10.1051/0004-6361:20020097, 2002.

Gunell, H., M. Holmström, E. Kallio, P. Janhunen, and K. Dennerl, X-rays from solar wind charge exchange at Mars, *Adv. Space Res.*, in preparation, 2004.

Hockney, R. W., and J. W. Eastwood, *Computer Simulation Using Particles*, IOP Publishing Ltd, Bristol, 1988.

Holmström, M., and E. Kallio, The solar wind interaction with Venus and Mars: Energetic neutral atom and X-ray imaging, *Adv. Space Res.*, *33*(2), 187–193, 2004.

Holmström, M., S. Barabash, and E. Kallio, X-ray imaging of the solar wind–Mars interaction, *Geophys. Res. Lett.*, *28*(7), 1287–1290, 2001.

Kallio, E., and P. Janhunen, Atmospheric effects of proton precipitation in the Martian atmosphere and its connection to the Mars-solar wind interaction, *J. Geophys. Res.*, *106*, 5617–5634, 2001.

Kallio, E., and P. Janhunen, Ion escape from Mars in a quasi-neutral hybrid model, *J. Geophys. Res.*, *107*(A3), 1035, doi: 10.1029/2001JA000090, 2002.

Kallio, E., J. G. Luhmann, and S. Barabash, Charge exchange near Mars: The solar wind absorption and energetic neutral atom production, *J. Geophys. Res.*, *102*, 22,183–22,197, 1997.

Keating, G. M., et al., The structure of the upper atmosphere of Mars: In situ accelerometer measurements from Mars Global Surveyor, *Science*, *279*(5357), 1672–1676, 1998.

Krasnopolsky, V., On the deuterium abundance on Mars and some related problems, *Icarus*, *148*, 597–602, 2000.

Krasnopolsky, V. A., and G. R. Gladstone, Helium on Mars: EUVE and PHOBOS data and implications for Mars' evolution, *J. Geophys. Res.*, *101*(A7), 15,765–15,772, 1996.

Schwadron, N. A., and T. E. Cravens, Implications of solar wind composition for cometary X-rays, *The Astrophysical Journal*, *544*, 558–566, 2000.

Shapiro, V. D., R. Bingham, J. M. Dawson, Z. Dobe, B. Kellet, and A. Mendis, Energetic electrons produced by the lower hybrid waves in the cometary environment and soft X-ray emission: Bremsstrahlung and K-shell radiation, *J. Geophys. Res.*, *104*, 2537, 1999.

Wegmann, R., H. U. Schmidt, C. M. Lisse, K. Dennerl, and J. Englhauser, X-rays from comets generated by energetic solar wind particles, *Planetary and Space Science*, *46*(5), 603–612, 1998.

H. Gunell, Swedish Institute of Space Physics, Box 812, SE-981 28 Kiruna, Sweden (herbert.gunell@physics.org)

M. Holmström, Swedish Institute of Space Physics, Box 812, SE-981 28 Kiruna, Sweden (matsh@irf.se)

E. Kallio, Finnish Meteorological Institute, Space Research, P.O. Box 503, FIN-00101 Helsinki, Finland (esa.kallio@fmi.fi)

P. Janhunen, Finnish Meteorological Institute, Space Research, P.O. Box 503, FIN-00101 Helsinki, Finland (pekka.janhunen@fmi.fi)

K. Dennerl, Max-Planck-Institut für extraterrestrische Physik, Giessenbachstraße, 85748 Garching, Germany (kod@mpe.mpg.de)